Bio-Design and Manufacturing (2026) 9:153–164
https://doi.org/10.1631/bdm.2500013

RESEARCH ARTICLE

Microfluidic-templating fabrication of milli-capsules with ultrarigid and homogeneous shells for long-term retention and explosive release of water-soluble cargoes

Haoyue Zhang[1,3] · Qiaoxia Lin[1,3] · Zheng Zhang[1] · Tengfei Tian[1] · Chengze Li[1] · Chuanfeng An[1,4] · Kaiwen Chen[1] · Yonggang Zhang[1] · Rongming Liu[1] · Liya Liang[1] · Wei He[2,3] · Huanan Wang[1,2]

Received: 7 January 2025 / Accepted: 4 September 2025 / Published online: 15 January 2026

Abstract

Encapsulation of water-soluble cargoes in millimeter-sized capsules has enabled major advances in various fields, including pharmaceuticals, food, cosmetics, packaging, and materials. However, because of the lack of fabrication precision, low cargo retention, suboptimal mechanical properties, and difficulty in preventing water evaporation, this technique is more challenging than microencapsulation techniques. In this study, we developed a surfactant-free and organic solvent-free water-in-oil-in-air emulsification approach for synthesizing double-layered "milli-capsules" for the precise encapsulation, enhanced retention, and force-triggered burst release of water-soluble bioactive cargoes. In particular, we synthesized milli-capsules with a first shell of poly(ethylene glycol dimethacrylate) for the efficient encapsulation of bioactive cargoes and a second shell of beeswax to prolong the retention of the entrapped bioactive compounds. Unlike traditional milli-capsules, which exhibit poor shape uniformity and mechanical stability, we introduced metallic ions to stabilize the interfacial tension and employed constant rotation to balance the gravity, buoyancy, inertial, and viscous forces imposed on the droplets, resulting in uniform and rigid milli-capsules with narrow rupture forces. Furthermore, additional hydrophobic beeswax coating prevented water volatilization and substantially prolonged the shelf life of the encapsulated compounds from a few days to a few months while maintaining their bioactivities. The proposed milli-capsule system addresses the challenge of precise fabrication of large carriers for water-soluble cargoes, representing a significant step toward the long-term storage and controlled release of bioactive cargoes for various industrial applications.

Haoyue Zhang and Qiaoxia Lin have contributed equally to this work.

✉ Huanan Wang
huananwang@dlut.edu.cn

[1] MOE Key Laboratory of Bio-Intelligent Manufacturing, Dalian Key Laboratory of Artificial Organ and Regenerative Medicine, School of Bioengineering, Dalian University of Technology, Dalian 116024, China

[2] State Key Laboratory of Fine Chemicals, Frontiers Science Center for Smart Materials Oriented Chemical Engineering, Dalian University of Technology, Dalian 116024, China

[3] School of Chemical Engineering, Dalian University of Technology, Dalian 116024, China

[4] Dalian Third People's Hospital, Dalian Eye Hospital, Dalian 116024, China

Graphical abstract

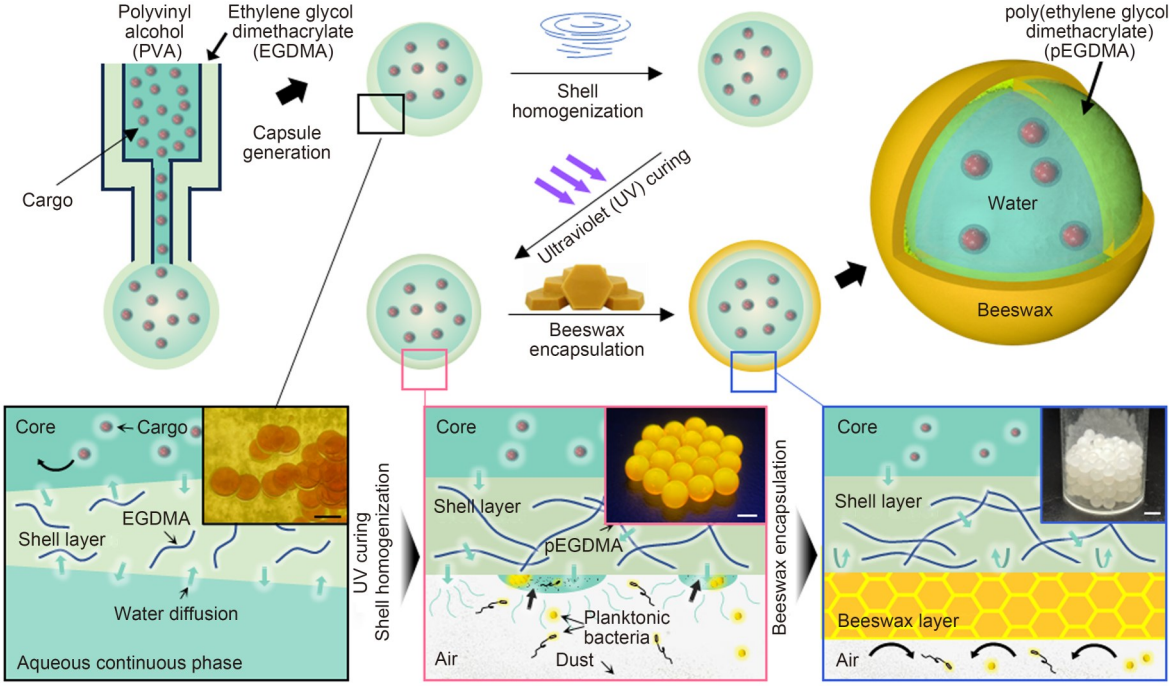

Keywords Droplet microfluidics · Millimeter-sized capsule · Double-emulsion droplet · Controlled release · Organic solvent-free encapsulation

1 Introduction

Encapsulation of bioactive cargoes in delivery vehicles has enabled significant advances in various fields, including pharmaceutical, food, cosmetics, packaging, and materials industries [1–3]. Millimeter-sized carriers with hydrophilic shells, such as gelatin, alginate, and starch, are the most widely adopted encapsulation systems in the pharmaceutical industry; however, they can only deliver hydrophobic ingredients, such as fish oil [4, 5], vitamins, curcumin [6], and various sweeteners [7]. Stable and controllable immobilization techniques for water-soluble, bioactive compounds in millimeter-sized capsules have not been extensively explored [8–16]. This can be attributed to the difficulty in inhibiting the water core volatilization. In particular, because many industrial applications require the entrapment of water-soluble cargoes for long periods [17–19], capsules with high mechanical and compositional stability are in increasing demand [20–22]. Milli-capsules made of hydrophobic polymer shells, such as poly(lactic acid) [23] and polystyrene [24], have been developed for the encapsulation of water-soluble cargoes [25, 26]. However, the synthesis of such hydrophobic polymer carriers involves techniques such as phase separation [27, 28] or solvent extraction [29], which are limited by the lack of precision in capsule fabrication and the potential cytotoxicity of the surfactant or organic solvent. Therefore, fabricating milli-capsules for water-soluble cargoes in a highly controlled and high-throughput manner without compromising the bioactivity and functionality of the payloads remains a challenge.

Recent progress in microfluidic techniques has enabled the fabrication of microcapsules in a highly controlled and continuous manner due to the advantages of fluid dynamics at the micrometer scale [30–32]. In contrast, the fabrication of milli-capsules with high controllability is challenging because of the more dominant influence of gravity and buoyancy on capsule sphericity and structural uniformity and the mismatch between the emulsion stabilization period and capsule polymerization rate [33–36]. To address these issues, previous studies have proposed the optimization of the existing fabrication strategies, such as using a multistep solidification strategy to ensure the integrity and mechanical properties of the shell layer [37], introducing an additional shell phase to enhance the encapsulation and retention efficiency of active biomolecules [17], and matching the densities of the core and shell phases to spontaneously form a uniform shell layer during the generation process [23, 38], which have enabled more controllable and high-throughput generation of milli-capsules. However, these optimization

methods have several bottlenecks, such as time- and cost-consuming fabrication due to the need for special generation methods, limited options for polymer shells due to the density matching requirement, and limited throughput. Therefore, there is still a need for highly controllable and high-throughput fabrication techniques for milli-capsule synthesis.

In this study, we developed a microfluidic-based, organic solvent-free and surfactant-free double-emulsion system to synthesize water-core milli-capsules for the prolonged encapsulation and force-triggered burst release of bioactive payloads. In particular, ultraviolet (UV)-polymerizable poly(ethylene glycol dimethacrylate) (pEGDMA) capsules with millimeter-sized monodispersity, a uniformly distributed shell layer, and fine-tunable rupture forces were fabricated using a specifically designed three-dimensional (3D)-printed co-flow microfluidic device (Figs. 1a and 1b) [39]. To address the difficulty in obtaining uniform polymeric shells with traditional fabrication techniques, we mediated the interfacial ion concentration to improve the interface stability of the double-emulsion system and introduced stirring to overcome the interruptions from the gravity effect, inertial, and viscous forces, resulting in uniform and rigid milli-capsules with tailorable compressive forces to rupture the capsules and enable cargo release (Figs. 1c and 1d). By introducing a secondary hydrophobic beeswax shell, the shelf time of the encapsulated water-soluble cargoes was significantly prolonged from a few days to a few months without extensive volatilization (Fig. 1e). This microfluidic templating strategy offers an innovative and cost-efficient approach for synthesizing milli-capsules for the immobilization and storage of water-soluble and bioactive cargoes, making them suitable for various applications in the pharmaceutical, food, and packaging industries.

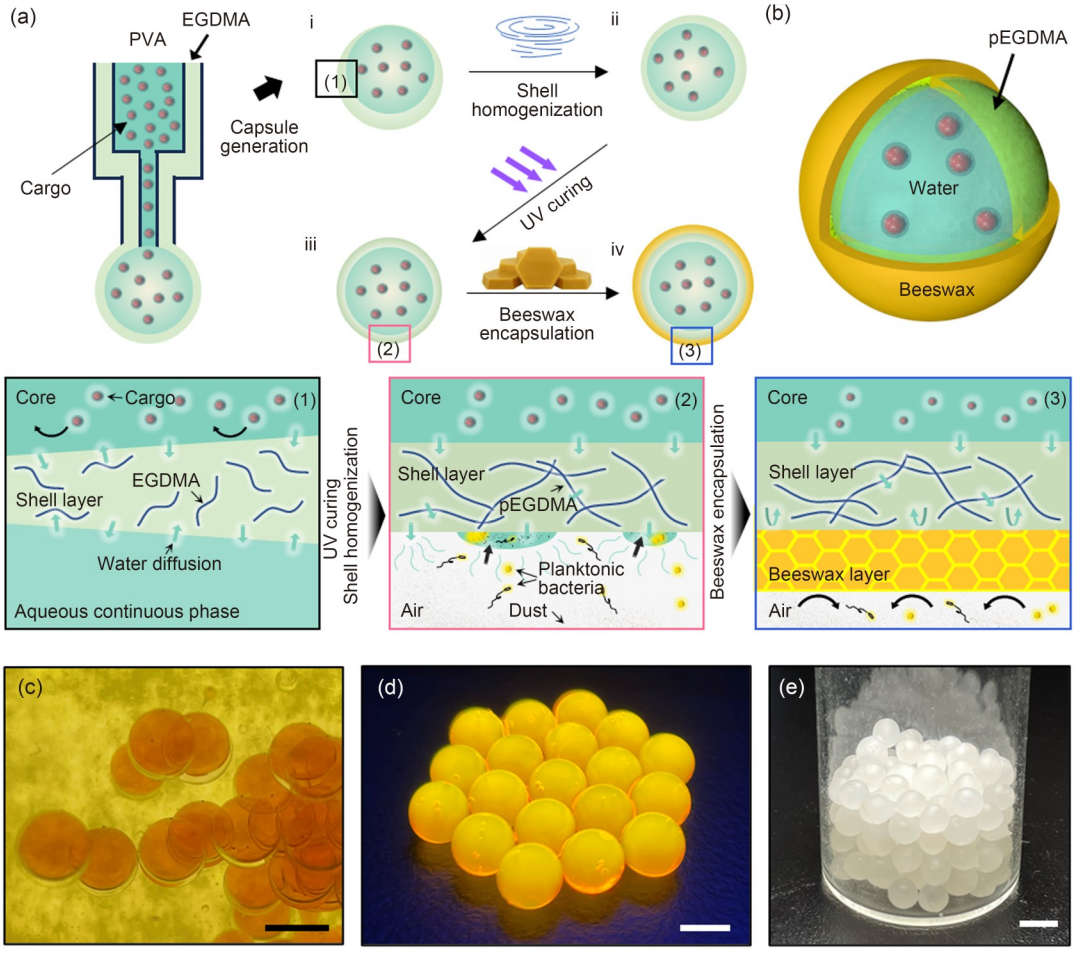

Fig. 1 Schematics for the production of homogeneous and rigid capsules with a rigid and impermeable shell for the encapsulation and storage of liquid-phase bioactive cargoes. (a) Core–shell capsules are first formed in air from a nested double-tube nozzle (i, (1)), and are made uniform in shell thickness through the shell homogenization process in aqueous continuous phase (i–ii). Then, the shell phase is photopolymerized to form the rigid shell (ii–iii, (2)), and finally encapsulated by a beeswax shell (iii–iv, (3)). (b) Schematic illustration of a rigid capsule encapsulated by beeswax. (c) The photograph of W/O/W core–shell double-emulsion droplets in aqueous continuous phase before photopolymerization. (d) Fluorescent photograph of capsules with a rigid shell and a water core. The water core is marked by Eosin Y. (e) A photograph of the rigid capsule encapsulated by beeswax. Scale bars: 3 mm. PVA: polyvinyl alcohol; W/O/W: water-in-oil-in-water

2 Results and discussion

2.1 Synthesis of water-core milli-capsules with pEGDMA shell via water-in-oil-in-air (W/O/A) double emulsion using 3D-printed microfluidic devices

Traditional strategies employ water-in-oil-in-water (W/O/W) emulsions to synthesize water-core capsules with enhanced cargo retention [3, 11] and require surfactants to stabilize the droplets. However, cost- and labor-intensive demulsification and washing are required to remove the residual surfactant, which may affect the functions or bioactivity of the cargoes [40, 41]. To address these issues, we propose a surfactant-free W/O/A emulsion (Fig. 2a) for synthesizing capsules with water cores and polymer shells [17, 42]. Droplet generators with channel dimensions of hundreds of microns were integrally fabricated via digital light processing to form core–shell droplets [30, 39]. The device, designed to mix aqueous and oil phases, comprises two coaxial tubular channels connected to separate inlets. The output of the device aligns perpendicularly to a water pool, allowing droplets to be pinched off by the force of gravity and collected downstream in water, followed by UV irradiation to polymerize the ethylene glycol dimethacrylate (EGDMA) phase (Fig. 2a; Fig. S1 in the supplementary information). A liquid containing EGDMA monomers and 1% (mass fraction) photoinitiator (2-hydroxy-2-methylpropiophenone) was used as the oil phase to generate double-emulsion droplets, and a 5% (mass fraction) polyvinyl alcohol (PVA) aqueous solution was used as the inner phase, with PVA acting as a surfactant to stabilize the water/oil interface [5, 43]. The two liquids were introduced into the droplet generator to allow the formation of a coaxial fluid.

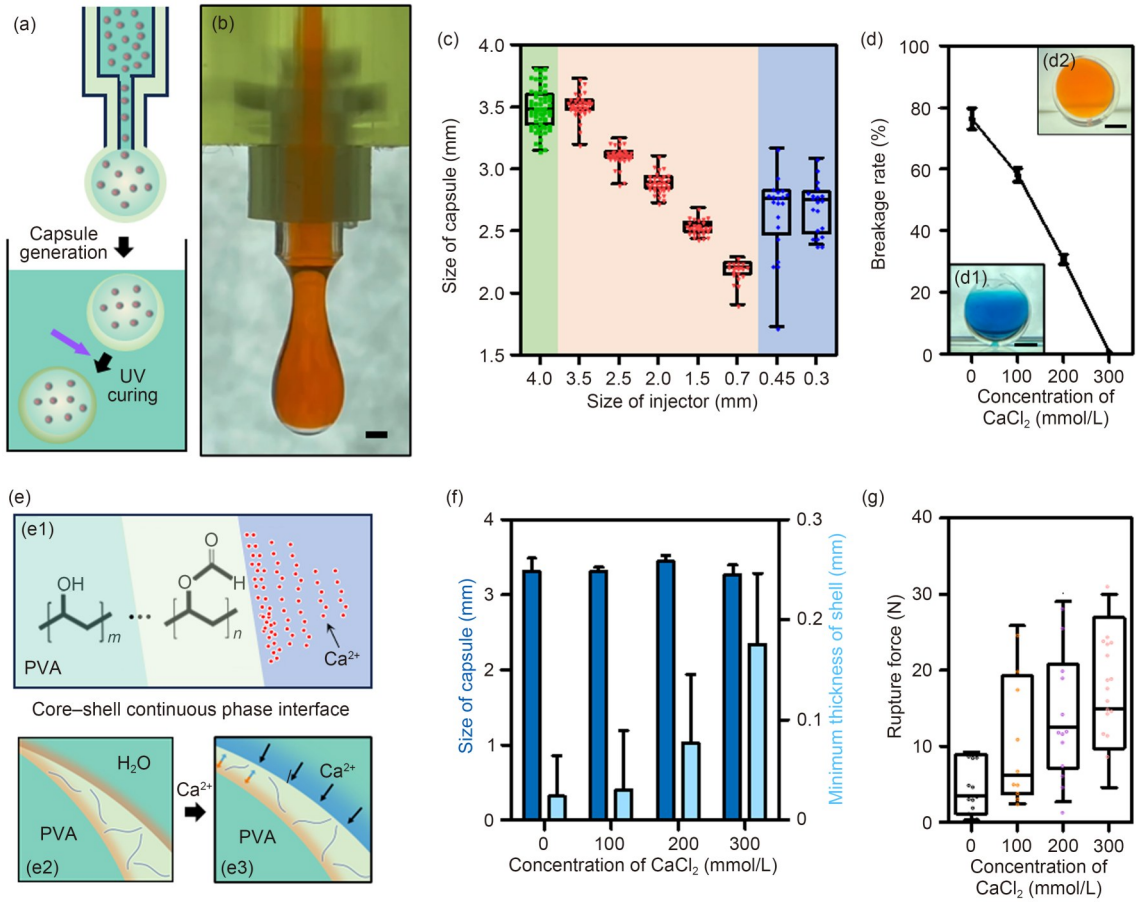

Fig. 2 Production and optimization of rigid capsules using double-emulsion droplets. (a) Schematic of the rigid core–shell capsule production process. (b) Photograph of the water-in-oil-in-air (W/O/A) core–shell droplet production using a nested double-tube nozzle. Scale bar: 1 mm. (c) Size distribution of the obtained core–shell capsules as a function of nozzle size. (d) Breakage rate of the rigid capsules as a function of cation introduction and the fractured (d1) and intact (d2) capsule products. Scale bars: 1 mm. (e) Schematic of the ion concentration effect strategy. Calcium ions in aqueous solution exhibit a more significant enrichment on the saline side of the interface (e1). Thus, the introduction of cations can improve the repulsive effect between the internal and external interfaces of the shell phase (e2 to e3). Size distribution and minimum shell thickness (f) and rupture force (g) of the resulting core–shell capsules as a function of cation concentration. Data in (c, d, f, g) are expressed as mean±standard deviation (n=30)

The co-flow fluids were immediately broken into stable and monodisperse W/O/A double-emulsion droplets upon injection into the continuous air phase (Fig. 2b; Fig. S3a in the supplementary information).

The formation of double-emulsion droplets was dominated by the interfacial tensions within the W/O/A system, which can be described using the spreading coefficients as follows [17, 42]:

$$S_i = \gamma_{j,k} - \gamma_{i,j} - \gamma_{i,k}, \quad (1)$$

where $\gamma_{a,b}$ is the interfacial tension between phases a and b. The spreading coefficient (S_i) indicates the propensity of a middle fluid (i) to spread between the two other immiscible fluids (inner phase, j, and the outer phase, k). $S_i>0$ indicates that the intermediate fluid spontaneously spreads between the other two fluids, forming a stable core–shell droplet. In contrast, $S_i<0$ indicates that the intermediate fluid separates from the internal fluid, forming two independent droplets. In the proposed W/O/A emulsion system, the spreading coefficient of the oil phase (S_O=10.22 mN/m; Table 1) allows the oil phase to remain stable by engulfing the water drop, forming core–shell double-emulsion droplets dispersed in the air (Fig. S3 in the supplementary information). However, for a W/O/W double-emulsion system, the interfacial tension between the two aqueous phases was too small to measure. Thus, the spreading coefficient S_O of the W/O/W double-emulsion system was less than 0, and a stable core–shell droplet could not spontaneously form.

Table 1 Interfacial tension between different phases, measured using the pendant drop method

Interface	γ (mN/m)
EGDMA–water	11.02
EGDMA–5% PVA solution	6.51
Air–EGDMA	37.72
Air–water	74.41
Air–10% PVA solution	54.45

Upon droplet formation, a balance between gravity and interfacial tension can be achieved (Fig. S4a in the supplementary information) [44, 45], enabling the continuous formation of monodisperse double-emulsion droplets with a coefficient of variation (CV) for droplet sizes of <3% (Fig. 2c). The droplet size can also be modified using the nozzle size of the droplet generator. For instance, a 2-mm diameter nozzle can produce capsules with an average size of (2.89±0.09) mm. As the nozzle diameter increased from 0.7 to 3.5 mm, the droplet size increased from (2.18±0.09) mm to (3.52±0.10) mm. However, due to the excessive wetting of the liquid phase on the nozzle surface or the insufficient interface force, the two liquid phases could not form stable plug-like droplets on nozzles >3.5 mm or <0.7 mm, making it difficult to prepare capsules with controlled sizes ((3.49±0.16) mm for nozzle size of 4 mm and (2.65±0.32) mm for nozzle size of 0.45 mm; Fig. 2c; Fig. S4 in the supplementary information).

2.2 Synthesis of capsules with intact polymer shells

After collecting the core–shell droplets in water, buoyancy plays a role due to the density difference between the water and oil phases, which can significantly impact the droplet stability and the integrity and uniformity of the polymer shells of the milli-capsules. In particular, because of the liquidity of EGDMA monomers and the density difference between the core and shell phases, the capsule shell layer was nonuniform, with one side typically thinner than the other (Fig. S5a in the supplementary information). Under static conditions, the nonuniform shell did not significantly affect the stability of the double emulsion due to interfacial tension (Fig. 1c). However, upon UV irradiation, the polymerization of EGDMA in the oil phase could cause volumetric shrinkage of the shell and introduce internal stress at the interface, thereby disrupting the interfacial stability. This resulted in the breakage of the emulsion droplets and the formation of incompletely closed capsules (Fig. 2d).

To address this issue, we enhanced the interfacial tension of the inner and outer interfaces of double-emulsion droplets to prevent capsule rupture upon EGDMA polymerization. Previous studies have demonstrated that the enrichment of divalent ions at the interface can provide a negative electrostatic potential to the brine-rich side and a positive electrostatic potential to the other side of the interface (Fig. 2e) [46]. Therefore, the metallic ion concentration at the interface can generate a repulsive effect between the brine-rich water phase and EGDMA-rich oil phase (Fig. 2e1) [47]. By adding Ca^{2+} to the outer aqueous phase in this double-emulsion system, the interfacial tension between the middle oil and outer aqueous phases was significantly improved (from (11.2±0.1) mN/m at 0 mmol/L Ca^{2+} to (13.9±0.3) mN/m at 100 mmol/L Ca^{2+}; Fig. S3d in the supplementary information). The metallic ion concentration at the interface also enhanced the repulsive effect between the outer brine-rich water and inner PVA phases. This is indirectly evidenced by the static contact angles between the salt solution and the PVA membrane surface, which increased from 67.43°±2.24° to 85.67°±0.91° as the ion concentration increased from 0 to 400 mmol/L (Fig. S5b in the supplementary information). The introduction of Ca^{2+} into the outer aqueous phase can induce a repulsive effect between the ion-rich and hydrophobic interfaces, significantly improving the interface stability of the capsules during polymerization.

The capsule morphology was observed to confirm the enhancement of the interface stability of the double droplets. Capsules formed without Ca^{2+} addition exhibited an average shell thickness of (0.023±0.020) mm. With the addition of 300 mmol/L Ca^{2+}, the average shell thickness of the pEGDMA capsules increased to (0.175±0.035) mm (Fig. 2f; Fig. S5c in the supplementary information), which addressed the issue of incompletely closed capsule formation due to less interfacial stability; the percentage of incompletely closed capsules decreased from (76.31±3.40)% to (0.47±0.02)% (Fig. 2d2). In turn, this improved the mechanical stability of the resulting capsules, as evidenced by the rupture force required to fracture the capsules increasing from (4.29±3.36) N to (19.69±6.40) N as Ca^{2+} increased from 0 to 300 mmol/L (Fig. 2g).

2.3 Uniform milli-capsule shells by balancing the forces imposed on the droplets

Although the introduction of divalent ions can improve the interfacial stability and shell integrity of the resulting capsules, the influence of gravity and buoyancy of nonuniform milli-capsule shells remains a primary challenge, resulting in a wide deviation of the capsules' rupture force of (19.69±6.40) N (addition of 300 mmol/L Ca^{2+}) with a CV of 57.6% (Figs. 2g and 3a1; Fig. S6 in the supplementary information). To address this issue, we employed a simple strategy to produce double-emulsion droplets with a more uniform shell by collecting the droplets in an aqueous phase with continuous stirring, thereby introducing a nondirectional rotary flow on the droplet shell and balancing the buoyancy without changing the composition of the emulsion system (Figs. 3a and 3b). We deduced the underlying physical mechanism of this strategy to predict the impact of different rotation velocities on the droplet morphology (Fig. 3b). When the formed W/O/A droplets were dripped into the aqueous phase, four types of external forces were imposed on the droplets from the continuous phase: inertial force, viscous force, buoyancy generated by the density difference between the core and shell phases, and centrifugal force owing to the rotational flow. Consequently, the shear forces imposed on the droplets were presented as inertial stress $f_i \sim \rho u^2$, viscous stress $f_v \sim \eta u/L$, buoyancy $f_b \sim \Delta\rho g L$, and centrifugal stress $f_c \sim \Delta\rho u^2 L/R$, where ρ is the density of the shell layer, η the viscosity of the shell layer, $\Delta\rho$ the density difference between the core and the shell phases, u the rotational linear velocity of the capsules in the liquid, L the characteristic length of the shell layer, and R the motion radius of the droplets in the eddy. The key to producing droplets with homogeneous shell layers is to provide a suitable flow velocity to balance the various stresses. Accordingly, the inertial and viscous forces of the shell phase dominate the other forces, thereby lowering the impact of buoyancy ($\Delta\rho$). This requires the dimensionless variable $(f_i+f_v)/(f_b+f_c) > 1$ (Fig. 3c) [48]. Therefore, the rotational and linear velocities must be within a certain range (0.10–0.32 m/s) to ensure the dominance of viscous and inertial forces, thereby guiding the shell homogenization of double-emulsion droplets.

Based on this theory, we investigated the effect of rotational linear velocity on the homogenization of the capsules by varying the stirring rates. First, the shear forces generated by the rotary flows were weak, and the droplets were not significantly deformed, as revealed by no significant differences in the size distribution of the capsules produced at different stirring rates (Fig. S7 in the supplementary information). The rupture forces of the capsules produced at different stirring rates exhibited a trend similar to that of the aforementioned dimensionless variables (Figs. 3c and 3d). In particular, there was no significant change in the average force required to rupture the solidified capsules as the stirring rate increased from 0 to 180 r/min. However, the distribution of the forces gradually narrowed with increasing stirring rates, with the CV decreasing from 57.6% to 19.8% as the stirring rate increased from 0 to 180 r/min. These results indicate that the shear forces imposed on the core–shell droplets gradually balanced as the stirring rate increased to 180 r/min. In contrast, as the stirring rate further increased, the distribution of rupture forces began to widen, with the CV increasing to 56.6% as the stirring rate reached 300 r/min. This result can be attributed to the excessively increased centrifugal force, which gradually disrupted the balance between the different forces on the droplets (Fig. 3c). Based on this approach, we optimized the stirring rates for homogeneous shell formation, as revealed by the relatively narrow distribution of the rupture forces (Fig. 3d) and a more uniform shell structure (Figs. 3e2 and 3f2).

Furthermore, we tested the effectiveness of this approach in fabricating milli-capsules with different shell thicknesses. The thickness of the milli-capsules was fine-tuned by mediating the flow rate ratio between the inner water-core phase (Q_c) and the oil phase of the EGDMA monomer (Q_s) (Fig. 3g). However, the change in the flow rate ratio can directly affect the volume fraction of the shell layer in the capsule, thereby affecting the characteristic length L of the shell and allowing buoyancy and centrifugal forces to play a more dominant role. Consequently, the stirring speed should be adjusted for capsules formed at different flow rate ratios, Q_s/Q_c, as evidenced by the rupture forces required to break the capsules with different shell thicknesses. The shell thickness of the milli-capsules increased with Q_s/Q_c. However, at the same stirring rate (180 r/min), varying degrees of homogenization of the shell layer were observed, as revealed by the wide distribution of the fracture force for the resulting capsules (Fig. 3h). This strategy allowed the production of milli-capsules with a more uniform shell thickness that can adapt to practical application scenarios,

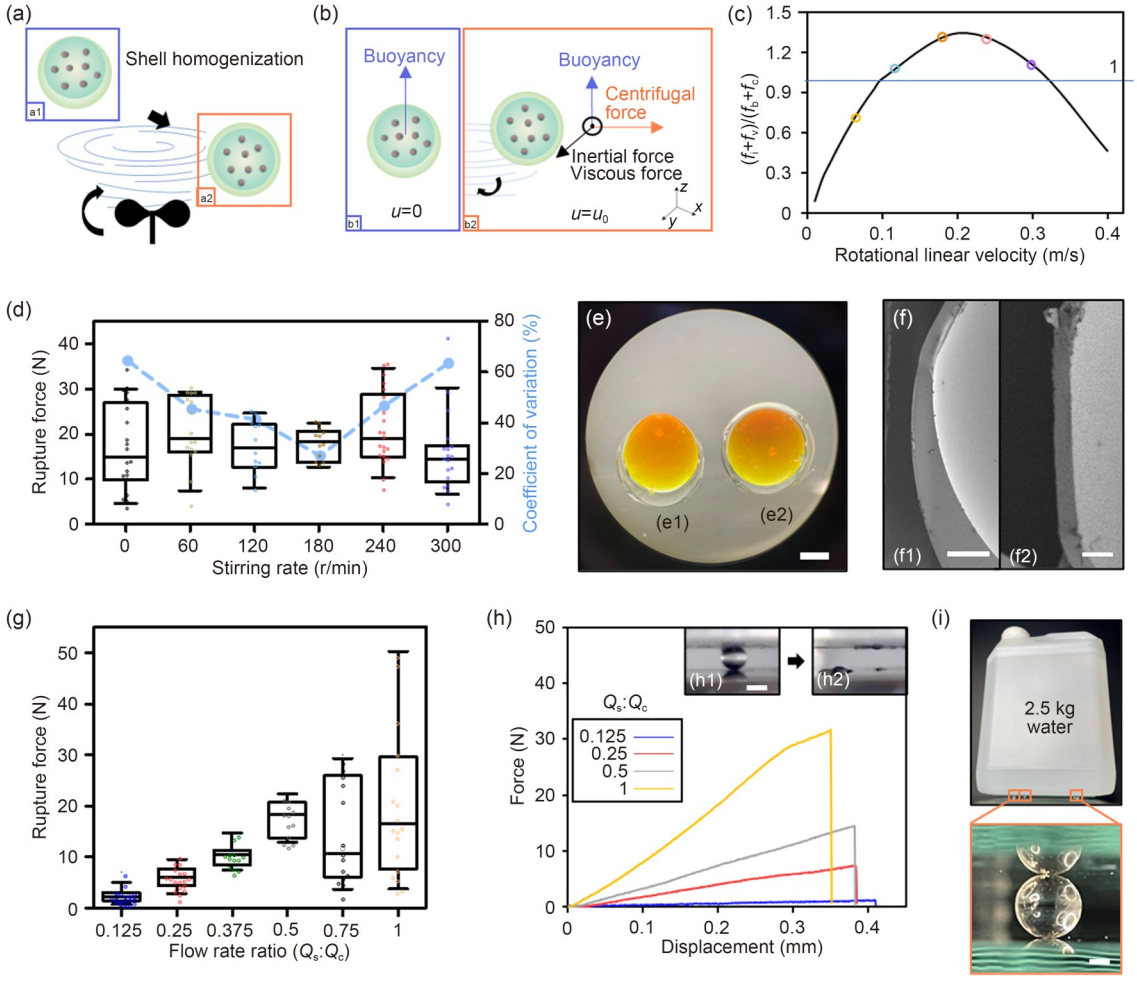

Fig. 3 Shell homogenization process for the rigid capsules. (a) Schematic of the shell homogenization process for the rigid core–shell capsules. (b) Forces in the single-core double-emulsion formation mechanism. In the static continuous phase, the density difference between the core and shell phases causes the core to float and form an eccentric capsule (b1). In the dynamic continuous phase, both the core and shell phases gain inertial and viscous forces. Under this domination, the influence of buoyancy can be reduced during the capsule formation process (b2). (c) Dimensionless quantification of the comparison between forces that govern the capsule generation. A value larger than 1 indicates the dominance of inertial and viscous forces for capsules. (d) Rupture force distribution of the resulting core–shell capsules as a function of stirring rate. (e) Photographs of the rigid capsule without (e1) and with (e2) the shell homogenization process. Scale bar: 1 mm. (f) Scanning electron microscopy (SEM) images of the capsule shell without (f1) and with (f2) the shell homogenization process. Scale bars: 500 μm. (g) Rupture force of the resulting core–shell capsules as a function of the flow rate ratio of the shell (Q_s) to that of the core (Q_c) phases at a fixed Q_c (20 mL/h). (h) Force–displacement curves for the core–shell capsules fabricated under different Q_s/Q_c ratios at a constant Q_c of 20 mL/h. Still-shot images of rigid capsules before (h1) and after (h2) crushing. Scale bar: 3 mm. (i) Representative photographs showing the intensity of the rigid capsules, with 2.5 kg of water sustained by four rigid capsules. Scale bar: 1 mm. Data in (d, g) are expressed as mean±standard deviation (n=30)

such as 6–21 N for cigarette capsules, thereby enabling more stable mechanical performance of the resulting capsules, as evidenced by four individual milli-capsules weighing 2.5 kg each (Fig. 3i).

2.4 Long-term retention of water-soluble cargoes within milli-capsules by introducing a second shell of beeswax

Another critical limitation of the application of water-core capsules is the uncontrollable volatilization of the water core in an ambient environment (Fig. 1a-2). Despite being hydrophobic (hydrophobic parameter, XlogP=1.9), the pEGDMA capsule shell was insufficient to limit the volatilization of water molecules. The weight loss rate of the pEGDMA milli-capsules reached (4.53±0.46)% (mass fraction) within two days at room temperature (20 °C) and 40% relative humidity (RH) and (70.47±2.35)% (mass fraction) in an extremely dry environment (37 °C; 5% RH; Fig. S8 in the supplementary information). Volatilization can compromise the activity and functionality of encapsulated cargoes during long-term storage.

To reduce the volatilization of moisture content from the water core, we introduced a secondary shell layer composed

of biocompatible beeswax. Inspired by interface-crossing encapsulation strategies [49–51], we prepared a molten beeswax reservoir floating on top of a cold alcohol solution and coated the milli-capsules with a thin and dense wax layer upon dripping them into the alcohol solution (Figs. 4a and 4b). We tested the water retention of the double-shell milli-capsules. The mass loss of water cores after 28 d was significantly reduced to (1.05±0.01)% under normal conditions and (6.76±0.23)% in an extremely dry storage environment (Fig. 4c). This protective effect was sufficiently high that adding extra water-retaining components, such as glycerol, to the water core did not significantly enhance further anti-volatilization effects.

2.5 Long-term storage of bioactive cargoes with retained bioactivity and functionality

Capsules can be used for the long-term and robust storage of water-soluble and bioactive cargoes. Therefore, we encapsulated biomacromolecules, including bovine serum albumin (BSA) and green fluorescent protein (GFP), in the synthesized milli-capsules. We measured the retention of the encapsulated biomolecules under storage conditions with normal humidity (RH: 40%) but at different temperatures (4 °C and 20 °C). At both temperatures, the milli-capsules exhibited high BSA retention (>80%, mass fraction) after 28 d. The milli-capsules exhibited higher BSA retention at 4 °C ((95.8±1.5)%) than at 20 °C after 28 d (Fig. 4e). The encapsulated proteins maintained their activity, as revealed by the retained fluorescence of the entrapped GFP after 28 d. At 4 °C, the GFP fluorescent signals remained (82.3±1.2)% after four weeks of storage (Figs. 4d and 4e). These results indicate that the milli-capsules highly inhibit the volatilization of bioactive cargoes and retain their bioactivity and function.

Besides the storage of biomacromolecules, the synthesized capsules can be used to load and store living cells.

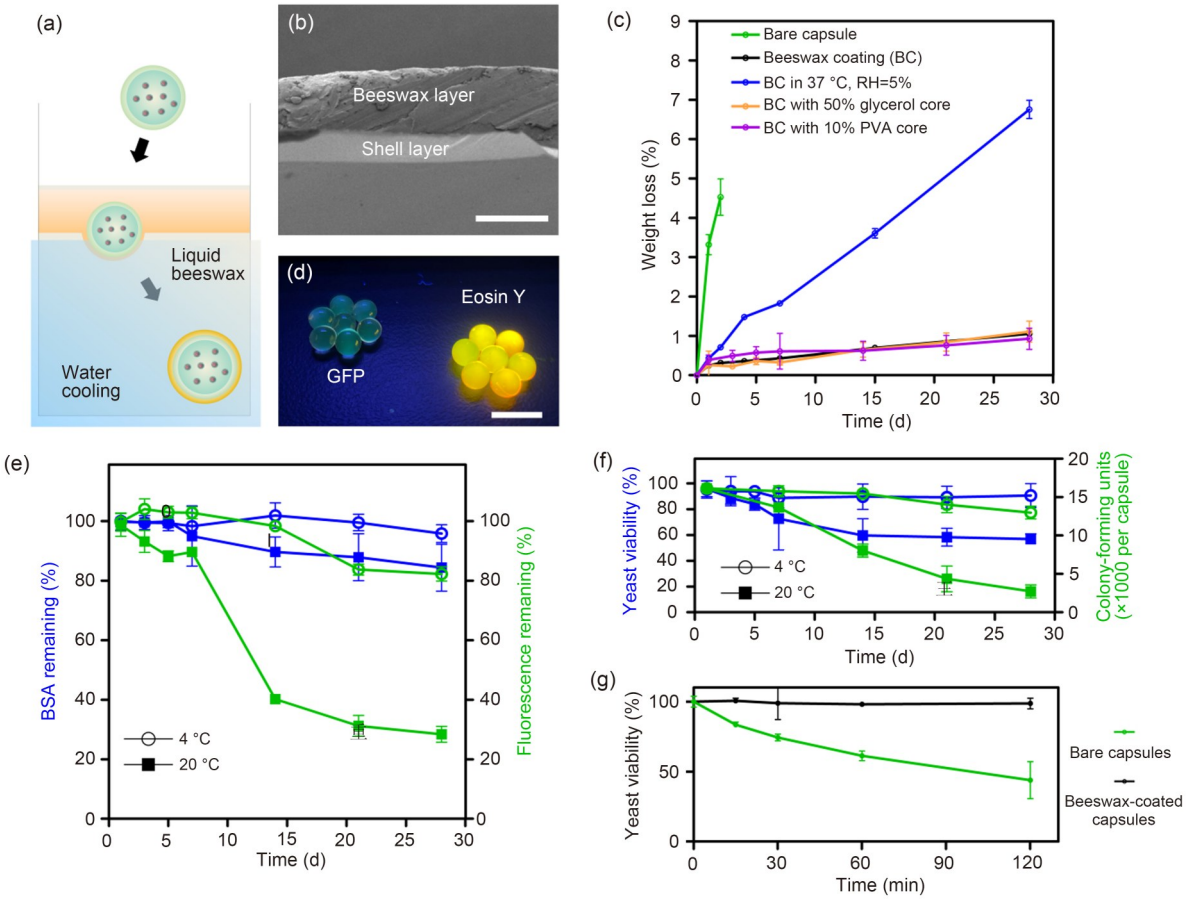

Fig. 4 Active substance encapsulation by rigid capsules with a beeswax layer. (a) Schematic of the beeswax-encapsulation process of the rigid core–shell capsules. (b) Representative SEM image of the attachment between the shell and beeswax layers. Scale bar: 500 μm. (c) Weight loss ratio of the coated core–shell capsules under different waterproof treatments. (d) Fluorescence photograph of the rigid core–shell capsules carrying green fluorescent protein and Eosin Y after 28 d. The water core was marked by Eosin Y. Scale bar: 5 mm. (e) BSA retention and residual fluorescence of the resulting core–shell capsules during storage. (f) Viability and colony-forming units of encapsulated yeasts during storage in air at different temperatures. (g) Viability of yeasts encapsulated in different capsules and stored in simulated gastric fluid. Data in (c, e–g) are expressed as mean±standard deviation (n=5)

Yeast cells encapsulated in rigid capsules retained their viability for 4 weeks under ambient conditions. After storage at 4 °C for one week, we observed a slight decrease in the viability of the encapsulated yeasts. However, the viability remained stable and then increased ((90.5±4.6)% cells) over the next three weeks of storage (Fig. 4f). This turning point can be attributed to the rapid dormancy of yeast at low temperatures. For the yeasts stored at room temperature, the viability continued to decrease in the first two weeks and remained stable in the last two weeks. The delayed turning point can be attributed to the slower dormancy of yeasts at higher temperatures. Further quantification of colony-forming units (CFUs) revealed a similar trend. When stored at 4 °C, the CFUs of the yeasts remained stable. However, that of the yeasts stored at room temperature continuously decreased for four weeks (Fig. 4f; Fig. S9 in the supplementary information).

The synthesized milli-capsules can also provide a strong protective effect against bioactive cargoes exposed to harsh gastric conditions. To confirm this, we stored the double-shell and bare pEGDMA milli-capsules in simulated gastric fluid at 37 °C for 2 h. The viability of the yeast cells encapsulated in the bare capsules significantly decreased, with only (43.9±6.5)% of cells remaining viable after 2 h of incubation (Fig. 4g). In contrast, the yeast encapsulated in the double-shell capsules maintained high viability ((98.7± 1.8)%), exhibiting negligible cell loss after 2 h of incubation. These results indicate that the synthesized milli-capsules can be used for the oral delivery of bioactive and fragile compounds; thus, they serve as promising, robust delivery systems for pharmaceutical and food industries.

3 Conclusions

In this study, we employed a microfluidic-based emulsification approach to synthesize double-layered, water-core milli-capsules with homogeneous and rigid shells for the encapsulation, long-term retention, and controlled release of water-soluble cargoes. Monodisperse pEGDMA milli-capsules with uniformly distributed shells and fine-tunable rupture forces were generated using customized 3D-printed microfluidic devices. Metal ions were introduced at the interface to improve the shell stability and structural integrity of the capsules. Capsules with a more uniform shell layer and enhanced mechanical stability were obtained by introducing a rotational flow to balance the various shear forces on droplets during shell polymerization. To address the issue of rapid volatilization of the water core, the rigid milli-capsules were coated with a secondary beeswax layer, which significantly prolonged the storage period and preserved the bioactivity of the encapsulated water-soluble cargoes. The obtained rigid capsules exhibited enhanced retention of water-soluble bioactive cargoes, promoting their application in the tobacco, cosmetics, and food industries. The synthesized rigid capsules also enable burst payload release and allow for time-of-demand and point-of-demand drug or substrate delivery, making them potentially beneficial in various fields, including chemistry, biology, and medicine.

4 Materials and methods

4.1 Materials

EGDMA, 2-hydroxy-2-methyl propiophenone, PVA, and glutaric dialdehyde were purchased from Sigma-Aldrich (USA). Beeswax, yeast extract, BSA, GFP, peptone, Eosin Y, agarose, glucose, and methylene blue were purchased from Solarbio (China). Photocurable resins were purchased from CREALITY (China) and BMF (China). Calcium chloride, glycerol, ethanol, isopropanol, and other chemicals were purchased from DAMAO (China).

4.2 Fabrication of microfluidic drive-pipe nozzles

For microfluidic chips with an injector size larger than 1 mm, chip devices were fabricated using our previously reported printing technology [39]. 3D models of chips (Fig. S1 in the supplementary information) were designed using Autodesk CAD (Autodesk Inc., San Rafael, CA, USA). BMF_3D slice (BMF Material Technology Inc., Shenzhen, China) and HALOT BOX (CREALITY, Shenzhen, China) were used to prepare the projection file. High-precision (nanoArch S140, wavelength 405 nm, BMF Material Technology Inc.) and large-scale 3D printers (LD-006, wavelength 405 nm, CREALITY) were used to print the inverted photocurable resin samples for parameter optimization (Fig. S1b in the supplementary information) and high-throughput generation of microfluidic devices (Figs. S1c and S1d in the supplementary information), respectively. The printed samples were washed with isopropanol for 30 min. The uncured resin remaining in the channel was removed by two washing steps with isopropanol. Subsequently, the microfluidic chip was rinsed with deionized water to remove isopropanol, and the remaining solvent was evaporated at 80 °C for 10 min.

For microfluidic chips with an injector size smaller than 1 mm, glass capillary microfluidic devices were used for testing. Cylindrical glass capillaries with an inner diameter of 560 μm (1B100-6, World Precision Instruments, Inc., USA) were used as the inner pipe, and square capillaries (Beijing Zhong Cheng Quartz Glass Co., Ltd., China) with an inner width of 1.05 mm were used as the outer pipe. Both capillaries were heated and pulled to fabricate nozzles with specific sizes using a micropipette puller (P-97, Sutter

Instrument, USA). The elongated capillaries were nested together to align the conical nozzles of the inner and outer pipes and then fixed with epoxy resin glue.

4.3 Computational fluid dynamics simulations

Commercially available software (COMSOL Multiphysics, COMSOL Co., Sweden) was used to simulate fluid dynamics in the microfluidic channels with different geometries (designed using AutoCAD, Autodesk Inc.). The minimal hydraulic pressure at the collection channel outlet was set to zero so that the hydraulic pressure values throughout the chip could be normalized by the maximal pressure at the aqueous phase inlet. Thus, the local fluid resistance was identical to the simulated fluid resistance. The flow rates of different liquids were used as input information for the simulation. Thus, we could obtain the heat maps of the hydraulic pressure (or fluid resistance) and flow velocity throughout the chip by simulation, in which the hydraulic pressure was calculated by the flow velocity at each position. The local fluid resistance and flow velocity for each drop maker unit (DMU) could be further quantified based on the heat maps. All computational fluid dynamics simulations based on the microfluidic chips of different geometries were performed using this setup.

4.4 Fabrication of rigid core–shell capsules

To generate core–shell double-emulsion droplets, the drive-pipe nozzle was hung above the aqueous continuous phase. A 10% (0.1 g/mL) PVA solution was used as the core phase, and EGDMA with 1% (0.01 g/mL) 2-hydroxy-2-methyl propiophenone was used as the shell phase. The core phase was injected into the inner pipe at a constant flow rate of 20 mL/h for each nozzle, and the shell phase was injected into the outer pipe at flow rates of 2.5, 5, 7.5, 10, 15, and 20 mL/h for each nozzle. A calcium chloride solution with varying concentrations (0, 100, 200, and 300 mmol/L) was used as the aqueous continuous phase (Fig. 2a). Core–shell double-emulsion droplets were formed as the droplets were pinched off the nozzle into the continuous air phase (Fig. 2b), after which the resulting W/O/A double-emulsion droplets were collected into an aqueous continuous phase (Fig. 1c). With continuous stirring at different rates, the droplets were further triggered to polymerize upon UV irradiation (300 mW/cm^2). After polymerization, the rigid milli-capsules were collected, washed three times with water, and dried with nonwoven fabric. After that, they were immersed in pure water for two days to remove the residual photoinitiator.

4.5 Mechanical stability tests

To investigate the mechanical properties of the synthesized rigid milli-capsules, compression tests were conducted using a universal testing machine (E43, MTS Instrument, USA) based on a previous report [33]. The capsules were meticulously aligned at the geometric center of the compression platens to minimize off-axis loading. The universal testing machine was programmed to execute displacement-controlled compression at a rate of 1 mm/min. For each group, at least 20 capsules were tested. To investigate the mechanical stability of the rigid capsules, four standard samples were sandwiched between two pieces of glass (10 cm×10 cm×0.5 cm), and a bucket containing 2.5 kg of water was placed on the glass (Fig. 3i).

4.6 Beeswax coating

The synthesized capsules were coated with beeswax to improve their cargo retention (Fig. 4a). Molten beeswax was continuously heated (65 °C) and floated on the upper layer of the water phase while the water phase was continuously cooled. The rigid capsules were dried with nonwoven and then vertically thrown into the molten beeswax. While the capsules fell through the beeswax layer due to gravity, they were coated with molten beeswax, which solidified upon cooling. Ethanol (30%, volume fraction) was added to the water phase to adjust its density so that the capsules with molten beeswax layer could be suspended in the water phase and capsules with solidified beeswax layer could sink to the bottom. Thereafter, the coated capsules were washed three times with water and stored in an ambient environment (20 °C, 40% RH). The microstructures of the beeswax coating and the polymer shell were observed using a scanning electron microscope (FlexSEM1000, Hitachi, Japan).

4.7 Proteins and yeast encapsulation and characterization

The storage of bioactive and water-soluble components, such as BSA (4 mg/mL), GFP (0.4 mg/mL), and yeast cells (10^6 cells/mL), was investigated by encapsulating them with the synthesized rigid capsules. The quantity (characterized by the retention of BSA) and quality (characterized by the retained GFP fluorescent signals) of the encapsulated bioactive macromolecules were evaluated at room temperature using a multimode microplate reader (SpectraMax M2e, Molecular Devices, USA). Rigid capsules were first crushed to release the core phase and diluted with an equal volume of water before the test. Yeast cells were cultured in extracted peptone dextrose (YPD) medium. The viability of the encapsulated yeasts was measured using methylene blue. To count the CFUs of the yeast in each capsule, the capsules were first crushed to release the yeasts. The cells were then plated on the yeast solid medium, and the CFUs were counted after 24 h. Five randomly selected capsules were used in each test.

4.8 Statistical analysis

All data are presented as mean±standard deviation. Data were analyzed using GraphPad Prism 5. Statistical differences were analyzed using one-way analysis of variance and Tukey's post hoc tests. A p value <0.05 was considered statistically significant.

Supplementary Information The online version contains supplementary material available at https://doi.org/10.1631/bdm.2500013.

Acknowledgements This study was supported by the National Natural Science Foundation of China (Nos. 52273102, 31870957, and 52302344), the Fundamental Research Funds for the Central Universities (Nos. DUT24YG155, DUT20YG103, and DUT22LAB601), and Liaoning Provincial Science and Technology Plan Joint Plan (No. 2023JH2/101700341). We thank the Home for Researchers editorial team for English language editing.

Author contributions HYZ and HNW designed the research. HYZ, QXL, ZZ, CZL, and CFA performed the experiments and analyzed the results. TFT, KWC, and LYL assisted in key experiments. HYZ, QXL, and WH wrote the manuscript. YGZ, RML, LYL, WH, and HNW provided funding support for this work. All authors commented on the manuscript.

Declarations

Conflict of interest HNW is an associate editor of *Bio-Design and Manufacturing* and was not involved in the editorial review or the decision to publish this article. The authors declare that they have no conflict of interest.

Ethical approval This article does not contain any studies with human or animal subjects performed by any of the authors.

Data availability The data that support the findings of this study are available from the corresponding author upon reasonable request.

Use of generative AI tools No generative AI tools were used in the preparation of this manuscript.

References

1. Zhao CX, Middelberg APJ (2011) Two-phase microfluidic flows. *Chem Eng Sci* 66(7):1394–1411. https://doi.org/10.1016/j.ces.2010.08.038
2. Zhao CX (2013) Multiphase flow microfluidics for the production of single or multiple emulsions for drug delivery. *Adv Drug Deliv Rev* 65(11/12):1420–1446. https://doi.org/10.1016/j.addr.2013.05.009
3. Li W, Zhang LY, Ge XH et al (2018) Microfluidic fabrication of microparticles for biomedical applications. *Chem Soc Rev* 47(15):5646–5683. https://doi.org/10.1039/C7CS00263G
4. Encina C, Vergara C, Giménez B et al (2016) Conventional spray-drying and future trends for the microencapsulation of fish oil. *Trends Food Sci Technol* 56:46–60. https://doi.org/10.1016/j.tifs.2016.07.014
5. Zhao CX, Chen D, Hui Y et al (2016) Stable ultrathin-shell double emulsions for controlled release. *ChemPhysChem* 17(11): 1553–1556. https://doi.org/10.1002/cphc.201600142
6. Nie B, Wang H, Rao CH et al (2021) Preparation and characterization of sodium alginate/phosphate-stabilized amorphous calcium carbonate nanocarriers and their application in the release of curcumin. *Nanotechnology* 32(37):375712. https://doi.org/10.1088/1361-6528/ac05ea
7. Xu C, Ban QF, Wang W et al (2022) Novel nano-encapsulated probiotic agents: encapsulate materials, delivery, and encapsulation systems. *J Control Release* 349:184–205. https://doi.org/10.1016/j.jconrel.2022.06.061
8. Seliktar D (2012) Designing cell-compatible hydrogels for biomedical applications. *Science* 336(6085):1124–1128. https://doi.org/10.1126/science.1214804
9. Galogahi FM, Zhu Y, An HJ et al (2020) Core–shell microparticles: generation approaches and applications. *J Sci Adv Mater Devices* 5(4):417–435. https://doi.org/10.1016/j.jsamd.2020.09.001
10. Moodie C, MacKintosh AM, Thrasher JF et al (2019) Use of cigarettes with flavor-changing capsules among smokers in the United Kingdom: an online survey. *Nicotine Tob Res* 21(11): 1547–1555. https://doi.org/10.1093/ntr/nty173
11. Datta SS, Abbaspourrad A, Amstad E et al (2014) 25th Anniversary Article: Double emulsion templated solid microcapsules: mechanics and controlled release. *Adv Mater* 26(14):2205–2218. https://doi.org/10.1002/adma.201305119
12. Sun JY, Zhao XH, Illeperuma WRK et al (2012) Highly stretchable and tough hydrogels. *Nature* 489(7414):133–136. https://doi.org/10.1038/nature11409
13. Nonoyama T, Gong JP (2021) Tough double network hydrogel and its biomedical applications. *Annu Rev Chem Biomol Eng* 12: 393–410. https://doi.org/10.1146/annurev-chembioeng-101220-080338
14. Tan HL, Guo S, Dinh ND et al (2017) Heterogeneous multicompartmental hydrogel particles as synthetic cells for incompatible tandem reactions. *Nat Commun* 8(1):663. https://doi.org/10.1038/s41467-017-00757-4
15. Jeong S, Nguyen HT, Kim CH et al (2020) Toward artificial cells: novel advances in energy conversion and cellular motility. *Adv Funct Mater* 30(11):1907182. https://doi.org/10.1002/adfm.201907182
16. Jambon-Puillet E, Jones TJ, Brun PT (2020) Deformation and bursting of elastic capsules impacting a rigid wall. *Nat Phys* 16(5): 585–589. https://doi.org/10.1038/s41567-020-0832-x
17. Lee H, Choi CH, Abbaspourrad A et al (2016) Fluorocarbon oil reinforced triple emulsion drops. *Adv Mater* 28(38):8425–8430. https://doi.org/10.1002/adma.201602804
18. Zieringer MA, Carroll NJ, Abbaspourrad A et al (2015) Microcapsules for enhanced cargo retention and diversity. *Small* 11(24): 2903–2909. https://doi.org/10.1002/smll.201403175
19. Kim SH, Kim JW, Kim DH et al (2013) Polymersomes containing a hydrogel network for high stability and controlled release. *Small* 9(1):124–131. https://doi.org/10.1002/smll.201201709
20. Zhu T, Jiang C, Wang ML et al (2021) Skin-inspired double-hydrophobic-coating encapsulated hydrogels with enhanced water retention capacity. *Adv Funct Mater* 31(27):2102433. https://doi.org/10.1002/adfm.202102433
21. Zhou C, So PS, Chen XW (2020) A water retention model considering biopolymer-soil interactions. *J Hydrol* 586:124874. https://doi.org/10.1016/j.jhydrol.2020.124874
22. Pérez-de-los-Reyes C, Sánchez-Ormeño M, Bravo Martín-Consuegra S et al (2022) The influence of depth on the water

retention properties of vineyard soils. *Agric Water Manag* 261: 107384.
https://doi.org/10.1016/j.agwat.2021.107384
23. Ekanem EE, Zhang ZL, Vladisavljević GT (2017) Facile microfluidic production of composite polymer core–shell microcapsules and crescent-shaped microparticles. *J Colloid Interface Sci* 498:387–394.
https://doi.org/10.1016/j.jcis.2017.03.067
24. Abbaspourrad A, Carroll NJ, Kim SH et al (2013) Polymer microcapsules with programmable active release. *J Am Chem Soc* 135(20):7744–7750.
https://doi.org/10.1021/ja401960f
25. Liu JY, Zhu MF, Shen ZH et al (2021) A polysulfides-confined all-in-one porous microcapsule lithium–sulfur battery cathode. *Small* 17(41):2103051.
https://doi.org/10.1002/smll.202103051
26. Kubiak T, Banaszak J, Józefczak A et al (2020) Direction-specific release from capsules with homogeneous or Janus shells using an ultrasound approach. *ACS Appl Mater Interfaces* 12(13):15810–15822.
https://doi.org/10.1021/acsami.9b21484
27. Haase MF, Brujic J (2014) Tailoring of high-order multiple emulsions by the liquid–liquid phase separation of ternary mixtures. *Angew Chem Int Ed* 53(44):11793–11797.
https://doi.org/10.1002/anie.201406040
28. Min NG, Ku M, Yang J et al (2016) Microfluidic production of uniform microcarriers with multicompartments through phase separation in emulsion drops. *Chem Mater* 28(5):1430–1438.
https://doi.org/10.1021/acs.chemmater.5b04798
29. Abate AR, Weitz DA (2009) High-order multiple emulsions formed in poly(dimethylsiloxane) microfluidics. *Small* 5(18): 2030–2032.
https://doi.org/10.1002/smll.200900569
30. Tsuda Y, Morimoto Y, Takeuchi S (2010) Monodisperse cell-encapsulating peptide microgel beads for 3D cell culture. *Langmuir* 26(4):2645–2649.
https://doi.org/10.1021/la902827y
31. Zhang WX, Qu LL, Pei H et al (2019) Controllable fabrication of inhomogeneous microcapsules for triggered release by osmotic pressure. *Small* 15(42):e1903087.
https://doi.org/10.1002/smll.201903087
32. Li YN, Yan D, Fu FF et al (2017) Composite core–shell microparticles from microfluidics for synergistic drug delivery. *Sci China Mater* 60(6):543–553.
https://doi.org/10.1007/s40843-016-5151-6
33. Lee SM, Hamonangan WM, Kim JH et al (2022) Soft and tough microcapsules with double-network hydrogel shells. *Adv Funct Mater* 32(34):2203761.
https://doi.org/10.1002/adfm.202203761
34. Chang CB, Wilking JN, Kim SH et al (2015) Monodisperse emulsion drop microenvironments for bacterial biofilm growth. *Small* 11(32):3954–3961.
https://doi.org/10.1002/smll.201403125
35. Wang JW, Hahn S, Amstad E et al (2022) Tailored double emulsions made simple. *Adv Mater* 34(5):e2107338.
https://doi.org/10.1002/adma.202107338
36. Liu XY, Steiger C, Lin ST et al (2019) Ingestible hydrogel device. *Nat Commun* 10(1):493.
https://doi.org/10.1038/s41467-019-08355-2
37. Lee H, Choi CH, Abbaspourrad A et al (2016) Encapsulation and enhanced retention of fragrance in polymer microcapsules. *ACS Appl Mater Interfaces* 8(6):4007–4013.
https://doi.org/10.1021/acsami.5b11351
38. Chen QS, Utech S, Chen D et al (2016) Controlled assembly of heterotypic cells in a core–shell scaffold: organ in a droplet. *Lab Chip* 16(8):1346–1349.
https://doi.org/10.1039/C6LC00231E
39. Luo ZM, Zhang HY, Chen RZ et al (2023) Digital light processing 3D printing for microfluidic chips with enhanced resolution via dosing- and zoning-controlled vat photopolymerization. *Microsyst Nanoeng* 9:103.
https://doi.org/10.1038/s41378-023-00542-y
40. An CF, Zhang YJ, Li HT et al (2021) Thermo-responsive fluorinated surfactant for on-demand demulsification of microfluidic droplets. *Lab Chip* 21(18):3412–3419.
https://doi.org/10.1039/D1LC00450F
41. An CF, Zhou RJ, Zhang HY et al (2023) Microfluidic-templated cell-laden microgels fabricated using phototriggered imine-crosslinking as injectable and adaptable granular gels for bone regeneration. *Acta Biomater* 157:91–107.
https://doi.org/10.1016/j.actbio.2022.11.034
42. Deng NN, Yelleswarapu M, Huck WT (2016) Monodisperse uni- and multicompartment liposomes. *J Am Chem Soc* 138(24): 7584–7591.
https://doi.org/10.1021/jacs.6b02107
43. Werner JG, Nawar S, Solovev AA et al (2018) Hydrogel microcapsules with dynamic pH-responsive properties from methacrylic anhydride. *Macromolecules* 51(15):5798–5805.
https://doi.org/10.1021/acs.macromol.8b00843
44. Montessori A, Lauricella M, Succi S et al (2018) Elucidating the mechanism of step emulsification. *Phys Rev Fluids* 3(7): 072202.
https://doi.org/10.1103/physrevfluids.3.072202
45. Stolovicki E, Ziblat R, Weitz DA (2018) Throughput enhancement of parallel step emulsifier devices by shear-free and efficient nozzle clearance. *Lab Chip* 18(1):132–138.
https://doi.org/10.1039/C7LC01037K
46. Li WH, Jin ZH (2019) Effect of ion concentration and multivalence on methane-brine interfacial tension and phenomena from molecular perspectives. *Fuel* 254:115657.
https://doi.org/10.1016/j.fuel.2019.115657
47. Mahmoudvand M, Javadi A, Pourafshary P et al (2021) Effects of cation salinity on the dynamic interfacial tension and viscoelasticity of a water-oil system. *J Petrol Sci Eng* 206:108970.
https://doi.org/10.1016/j.petrol.2021.108970
48. Zhu PG, Wang LQ (2017) Passive and active droplet generation with microfluidics: a review. *Lab Chip* 17(1):34–75.
https://doi.org/10.1039/C6LC01018K
49. Abkarian M, Loiseau E, Massiera G (2011) Continuous droplet interface crossing encapsulation (cDICE) for high throughput monodisperse vesicle design. *Soft Matter* 7(10):4610–4614.
https://doi.org/10.1039/C1SM05239J
50. Morita M, Onoe H, Yanagisawa M et al (2015) Droplet-shooting and size-filtration (DSSF) method for synthesis of cell-sized liposomes with controlled lipid compositions. *ChemBioChem* 16(14):2029–2035.
https://doi.org/10.1002/cbic.201500354
51. Kamiya K, Kawano R, Osaki T et al (2016) Cell-sized asymmetric lipid vesicles facilitate the investigation of asymmetric membranes. *Nat Chem* 8(9):881–889.
https://doi.org/10.1038/nchem.2537